Article

Microparticle Manipulation Based on the Bulk Acoustic Wave Combined with the Liquid Crystal Backflow Effect Driving in 2D/3D Platforms

Yanfang Guan,* Xiaoliang Wang, Guangyu Liu, Wujie Li, Kun Zhang, Baoshuo Sun, Feifan Shi, Yanbo Hui, Bingsheng Yan, Jie Xu, Zaihui Wu, Zhiyong Duan, and Ronghan Wei*

Read Online

ACCESS | Metrics & More | Article Recommendations

ABSTRACT: Microparticle manipulation has been widely used in clinical diagnosis, cell separation, and biochemical analysis via optics, electronics, magnetics, or acoustic wave driving. Among them, the bulk acoustic wave (BAW) driving method has been increasingly adopted because of non-contact, easy control, and precise manipulation. However, its low manipulation efficiency limits the usage of the BAW driving in high viscosity solutions. Therefore, in order to obtain larger driving force and more flexible manipulation of microparticles, both two-dimensional (2D) and three-dimensional (3D) platforms based on the BAW and liquid crystal backflow effect (LCBE) driving in liquid crystal (LC) solutions are proposed. The driving forces applied on the microparticles allow for the change of microparticle moving direction, which is also ascertained through theory analysis combined with various driving methods. Specifically, the maximum moving speed (68.78 μm/s) of the polystyrene particles is obtained by the BAW (13 Vpp) combined with LCBE (30 V) at a low frequency of 7.2 kHz in the 2D platform. Precise position manipulation in 3D is also fulfilled through a programmable logic control model using polystyrene particles as a demonstration. In addition, red blood cells mixed with LC solutions are arranged in a line or gathered in the pressure nodes of the BAW forces along with sinusoid signals generated by various transducer combinations. Therefore, it is approved that the LC solution that induces the LCBE force could increase the microparticle manipulation efficiency in both 2D and 3D platforms. The proposed method will open up new avenues in particle manipulation and benefit a variety of applications in cell separation, drug synthesis, analytical chemistry, and others.
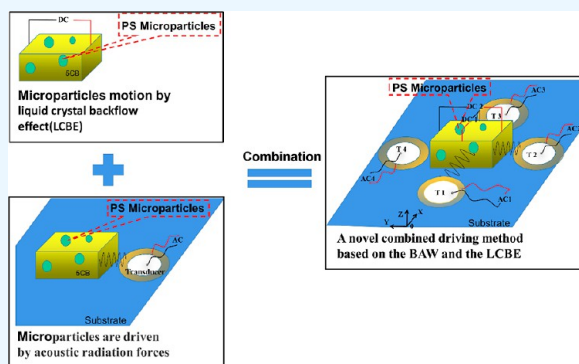
1. INTRODUCTION

For decades, microfluidic technologies have drawn significant attention due to advantages of miniaturization, portability, integration, automation, low cost, high throughput, and simple operation. As an interdisciplinary field, it combines the perspectives of chemistry, physics, life science, microelectronics, materials, computer science, and others and has been applied for in vitro diagnostic, liquid biopsy, environmental and biochemical analysis, single cell analysis, and nucleic acid analysis.[1] More specifically, regular analytical analysis steps such as mixing,[2] isolation,[3] enrichment,[4] manipulation,[5] sorting,[6] detection,[7] synthesis, and cell culture have been realized in small chips and microfluidic systems.

The ability of microfluidics to separate cells rapidly and efficiently often relies on external force fields, such as optics,[8] electronics,[9] magnetics,[10] or acoustics.[11−13] Among them, bulk acoustic wave (BAW)[14] manipulation based on acoustic streaming and radiation forces holds a great promise, as evidenced by its advantages, including versatility, biocompatibility, precision, flexibility, compactness, and cost-effective-

ness, as well as the ease of integration with other microfluidic technologies. So far, particles with a wide spectrum of size ranging from nanometers to millimeters in a variety of fluid media (e.g., air, whole blood, or sputum) are successfully manipulated using this technology.[15−19] Settnes and Bruus had analyzed the acoustic radiation force in detail on a compressible, spherical, micrometer-sized particle of radius suspended in a viscous fluid in an ultrasound field.[20] Dai et al. demonstrated that acoustic radiation forces and streaming induced by strong microfluidic oscillations at water−air surfaces of Helmholtz resonant air cavities at the topological interface capture microparticles, the sizes of which are up to 20
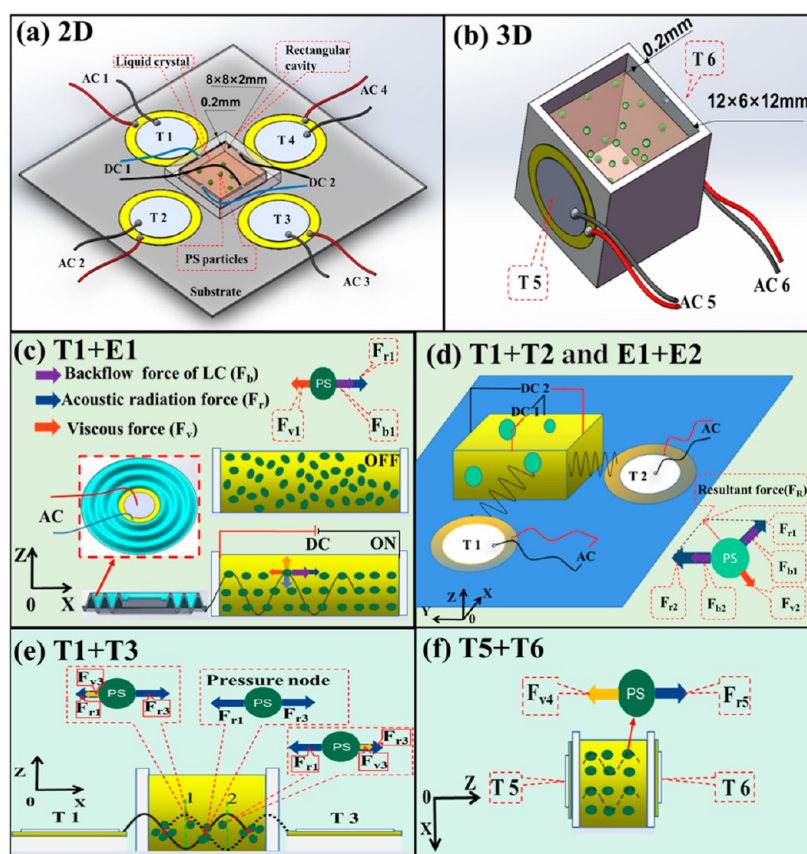
Figure 1. 2D and 3D platforms design and theory analysis of microparticles manipulation. (a,b) Dimensions of the 2D/3D platforms. (c) Manipulation principle of the microparticles (moving along *X* or *Y* directions) driven by one piezoelectric transducer combined with one DC electric field in the 2D platform. (d) Manipulation principle of microparticles (moving in *XOY* plane) driven by two adjacent piezoelectric transducers and two DC electric fields in the 2D platform. (e) Manipulation principle of microparticles (gathering in the pressure nodes in *XOY* plane) driven by two counter piezoelectric transducers in the 2D platform. (f) Manipulation principle of microparticles (moving in *YOZ* plane) by one transducer in the 3D platform.

μm, and make them undergo orbital rotations.[21] Moreover, in the field of regenerative medicine, Yu et al. had prepared materials containing living cells through microfluidics, an advanced engineering approach.[22] Yang et al. had presented a perspective of cellular fluidics-based construction of vascular networks for tissue engineering, with inspirations drawn from a novel concept of the 3D fluidic control platform based on unit-cell constructs.[23] Red blood cells (6−8 μm in diameter), one of the key indicators in clinical medicine, are isolated from the whole blood, which has important real-world implications because many biological targets span the same size range. For example, Huang et al. isolated exosomes from whole blood with a high blood cell removal rate in a microchannel by integrating high-frequency (39.4 MHz) interdigital transducers (IDTs).[24] Besides, they demonstrated an acoustofluidic platform that can code droplets by the focused interdigital transducers (FIDTs) with an optimal actuation frequency of 96.25 MHz.[25] Lee et al. optimized the design of the high-frequency (39.4 MHz) IDT and underlying electronics to isolate both nanoscale and microscale vesicles from cell culture media and achieved a high separation yield and resolution.[26] In addition, Huang et al. designed a simple, low-cost nature, and open fluidic chamber platform utilizing phase modulation between the two low-frequency (4−6 kHz) piezoelectric transducers to achieve dynamic particle concentration and the particle vortex translation.[27] This device based on the low-frequency piezoelectric transducer implemented only a single

direction operation of the particle vortex. However, the aforementioned particle manipulation methods relied on the high-frequency interdigital (IDT) driving transducers, which adopted the complicated fabrication process and high cost to limit the usage.

A liquid crystal (LC) is an ordered state between the liquid state and crystal state, which has the fluidity of liquid and sensitivity to the electric field.[28] A liquid crystal backflow effect (LCBE), owing to the rotation of LC molecules in the electric field, can drive the movements of liquid crystal molecules and other microparticles. In recent years, the research on liquid crystal mechanics has increased gradually, mainly focusing on the mechanical properties under electric and magnetic fields. For example, Liu developed a micro-fluidic actuator based on the liquid crystalline backflow. The velocity of the object is only 2 μm/s.[29] Guan developed a micropump based on a liquid crystal and piezoelectric transducers, with which the maximum flow rate achieved was 4.494 μL/min.[30] Liu demonstrated a one-dimensional model for a research of the control method based on the liquid crystalline backflow. The high drive quality can be achieved by fixing the rotation range of the molecules at the center of the cell within 50−80°.[31] However, downsides such as low driving force and small manipulation range limited the usage of the liquid crystal for particle manipulation.

Recently, there have been a lot of research about manipulation of particles in fluid media. Zhao et al.

demonstrated the pumping of water droplets based on capillary force[32] and developed and employed structural color micromotors (SCMs) that could realize multiplex label-free detection of ions based on their optical coding capacity and responsive behaviors.[33] As aforementioned, acoustic microfluidic methods can be integrated with other microfluidic designs for enhanced fluid and particle manipulation performance.[34−36] For example, Huang et al. achieved dynamic manipulation of micro-objects by combining hydrodynamic manipulation and acoustic microfluidic manipulation.[37−39] They developed acoustic circulating tumor cell (CTC) separation devices integrating hydrodynamics and IDT and isolated rare CTCs from peripheral blood in a single direction;[38] Zhou et al. presented a rapid and powerful method to size dependently control movement of microparticles and cells in paper using surface acoustic waves by combining paper-based microfluidics with acoustics.[40] Wang et al. proposed a generic single cell manipulation tool based on the integration of optical tweezers and microfluidic chip technologies for handling small cell population sorting with high accuracy.[41] These methods expanded the application scope to most types of microparticles but only deal with particle manipulation in a single direction.

In addition, as a high-viscosity solution, the liquid crystal can not only provide a weak driving force but also has excellent properties of dielectric anisotropy, which has a potential research value. Most of the current research is focused on the direction of liquid crystal display, and there are few studies on the driving direction of the liquid crystal microfluid. Combining the excellent performance of the liquid crystal with acoustic flow control overcomes the disadvantages (low driving force) of single actuation mode, manipulates microparticle random positions, and becomes more valuable for research.

In this paper, we presented a novel combined driving method based on the BAW and the LCBE driving to realize microparticle manipulation in liquid crystal solution. It uses low-cost, simple, low-frequency piezoelectric transducers to achieve flexible operation in 3D. The novel driving method is expected to achieve a larger displacement of particles (PS particles as a demonstration) in the LC solution under low driving voltage and frequency conditions. In addition, the new method can freely manipulate PS particles in the 2D/3D of the liquid crystal solution and enrich the red blood cell (RBC) near the pressure node using two counter transducers or the four transducers in the 2D platform. The FEA with the 3D platform under BAW driving has been obtained for the validation of the results. The results from both the numerical analysis and experiment show that the combined model is promising in cell separation, cell patterning, sample enrichment, reagent mixing, and manipulation of model organisms.

2. FABRICATION AND THEORY ANALYSIS

2.1. Design and Fabrication of Microparticle Manipulation Platforms.
The rectangular cavity with an inner size of 8 × 8 × 2 mm was designed as the 2D platform for microparticle manipulation. The glasses (0.2 mm of thickness) coated with indium tin oxide (ITO) conductive layer (0.2 μm of thickness), which will form direct current electric field (DC1 and DC2) between two counter glass sidewalls into the LC solutions, were selected as four sidewalls of the 2D platform. The PMMA substrate (45 × 45 × 0.1 mm) was fabricated using a laser engraving machine. Finally, the prepared sidewalls

and four piezoelectric transducers (T1, T2, T3, and T4) were bonded together and on the PMMA substrate using epoxy separately. In order to form the permanent connection and avoid leakage, the whole model was placed in the vacuum oven at 20 °C for 24 h. The structures and distribution of the 2D platform, in which four transducers were installed on the same substrates with the cavity, is shown in Figure 1a.

In the 3D platform, the piezoelectric transducers (T5 and T6) were fixed on the sidewalls of PMMA (0.2 mm of thickness) to form the cube with the size of 12 × 6 × 12 mm for microparticle manipulation, as shown in Figure 1b.

2.2. Theory Analysis.
Different driving mode combinations between BAW and LCBE will have an important influence on the microparticle. The direction and magnitude of velocity of microparticle movement will change according to the combination of BAW and LCBE. Thus, the theory analysis of microparticle forces include the direct current electric field (AC1 and AC2) and bulk acoustic wave (T1−T6, generated by transducer) combination in the 2D/3D platform. The detailed analysis is shown below.

2.2.1. Microparticle Movement Analysis with Different Driving Modes in the 2D Platform. 2.2.1.1. Piezoelectric Transducer (AC1) Combined with LCBE Electric Field (DC1). In this mode, the microparticles in LC solution are subjected to two forces, one is the acoustic radiation force (F_{r1}) generated by T1, which is mainly generated by traveling acoustic waves depending on the size and particles and enough input frequency (7 kHz), which is far lower than the frequency required by traveling acoustic waves to manipulate particles.[42] Another one is the LCBE force (F_{b1}) generated by DC1, as shown in Figure 1c. In addition, because of the microparticle movement, the viscous resistance force (F_{v1}) generated by the friction between PS particles and LC solution should be considered. Here, we neglect the gravity and buoyant force of PS particles because of their counter direction and similar magnitudes. Therefore, the moving direction of microparticles will be simplified and represented by the resultant between F_{r1}, F_{b1}, and F_{v1}. Note that the acoustic radiation force F_{r1} can be calculated by eq 1[43]

$$F_{r1} = -\left(\frac{\pi p_0^2 V \beta_\omega}{2\lambda}\right) \cdot \phi(\beta, \rho) \cdot \sin\left(\frac{4\pi x}{\lambda}\right) \tag{1}$$

where p_0 is the pressure amplitude, which depends on the amplitude of the acoustic wave; λ is the acoustic wavelength, which is constant for the same medium and frequency; V_c is the volume of the particle; x is the distance from a sidewall in the X/Y direction.

Here, $\phi(\beta,\rho)$ is the acoustic contrast factor that determines the direction of the acoustic radiation force. It can be calculated by eq 2[43]

$$\phi(\beta, \rho) = \frac{5\rho_c - 2\rho_\omega}{2\rho_c + \rho_\omega} - \frac{\beta_c}{\beta_\omega} \tag{2}$$

where ρ_c is density of the LC solution; ρ_ω is density of PS particles; β_ω is compressibility of medium; and β_c is compressibility of particles. Related parameters can be found in Table 1.

Here, ϕ increases with relative density and decreases with relative compressibility. Due to relatively higher density of PS than density of the medium, ϕ is positive.[39] In this research, six

Table 1. Parameters of the Liquid Crystal and PS Particles

content	value
density of PS particles/ρ_ω	1.05 g/cm^3
particle radius/r	10 μm
volume of the particle/V_c	41.8 cm^3
LC solution viscosity/η	32 Pa·s
LC rotational viscosity/γ_1	229 Pa·s
density of LC solution/ρ_c	1.008 g/cm^3
electric permittivity/$\varepsilon_\parallel$	15.7 × 10^{11} F/m
and $\varepsilon_\perp$	5.7 × 10^{11} F/m
temperature/T	300 K

piezoelectric transducers are the same, which will generate identical acoustic waves.

In the literature,[29] the liquid crystal solution will generate the small motion along with the direct current (DC) electric field direction under liquid crystal backflow effect (LCBE) force. Therefore, the microparticles mixed into the LC solution can be manipulated by changing the DC parameters. The LCBE force F_{b1} caused by direct current electric field is calculated by eq 3[30]

$$F_{b1} = [(\varepsilon_\perp E + \varepsilon_\alpha (n \cdot E) n \cdot \nabla)]E \tag{3}$$

where ∇ is the Hamilton operator; n is the direction vector; E is the electric field intensity generated by DC1; and ε_α is the dielectric anisotropy of the liquid crystal, which can be

expressed as the difference between the dielectric constant of the liquid crystal in eq 4

$$\varepsilon_\alpha = \varepsilon_\parallel - \varepsilon_\perp \tag{4}$$

where $\varepsilon_\parallel$ is parallel to the direction vector n, and the dielectric constant of the liquid crystal $\varepsilon_\perp$ is perpendicular to direction vector n. The value can be found in Table 1. E is the field strength of the electric field, which is calculated by eq 5

$$E = U/d \tag{5}$$

where U is the voltage applied on DC1or DC2; d is the distance between two electrodes in the direction of field strength.

The viscous resistance force F_{v1} can be calculated by eq 6[44]

$$F_{v1} = -6\pi\eta r v \tag{6}$$

where η is LC solution viscosity. r is the PS particles radius, and v is relative velocity.

Therefore, the total force $\sum F_1$ applied on the PS microparticles driven by T1 and DC1 was calculated in eq 7 and is shown as follows

$$\sum F_1 = F_{r1} + F_{b1} - F_{v1} \tag{7}$$

That can be attributed to ordered arrangement of the PS particles resulted from rotation of LC molecules in the DC electric field.[31] The LCBE force of LC solution carries PS particles moving under the DC field. Because the sum of F_{r1} and F_{b1} is larger than F_{v1}, thus PS particles move in +X
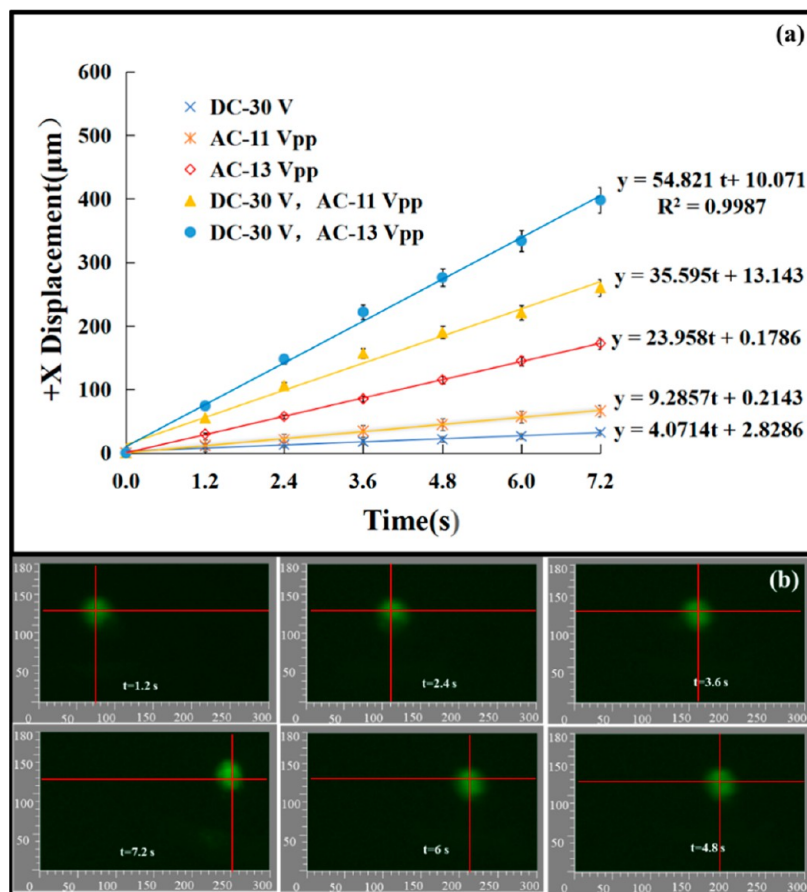
Figure 2. Motion analysis of PS particles with different BAW and LCBE combination driving mode. (a) Time-displacement curve of PS particles in +X directions with single BAW or/and LCBE driving modes. (b) Motion trajectories of PS particles by LCBE and BAW combined driving.
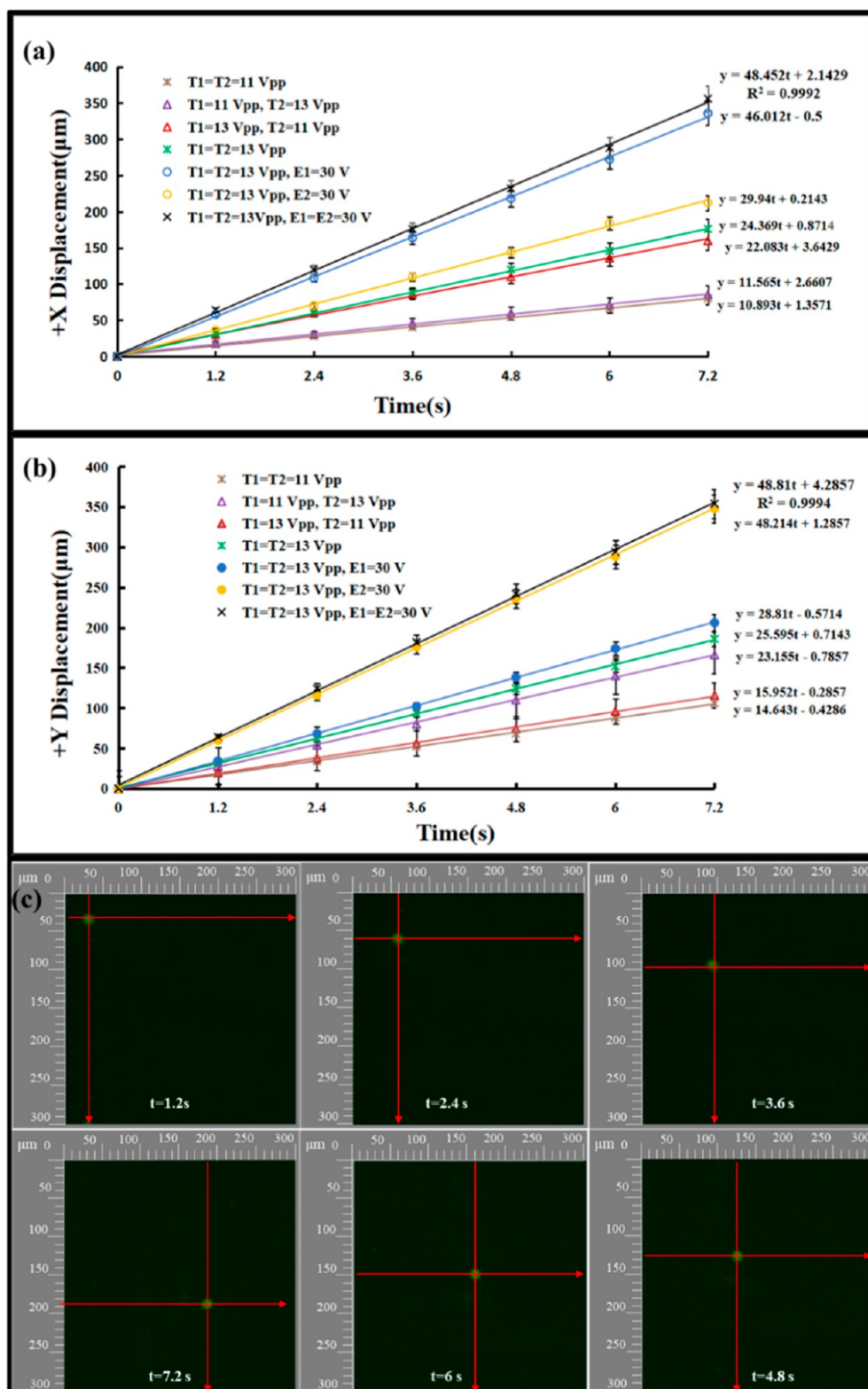
Figure 3. Experiment analysis of microparticle manipulation with different T1, T2, E1, and E2 driving combination. (a,b) Time displacement curves of PS particles in the +X/+Y direction at different driving mode combinations. (c) Motion trajectories of PS particles at T1 = 13 V and T2 = 13 V.

direction. The higher the particle velocity (v), the greater the viscous force (F_{v1}). When $\sum F_1$ is equal to zero, the velocity of the PS particles remains constant. Consequently, the velocity of microparticles will have different velocity under different driving voltages according to eqs 1−7.

2.2.1.2. Two Piezoelectric Transducers (AC1 + AC2) Combined with Two LCBE Electric Field (DC1 + DC2). In this case, the forces applied on the PS microparticles include acoustic radiation forces F_{r1} and F_{r2} generated by piezoelectric transducers 1 and 2, the LCBE forces F_{b1} and F_{b2} generated by

DC1 and DC2, and the viscous resistance force F_v, as shown in Figure 1d. Similarly, the total force $\sum F_2$ applied on PS particles can be calculated by eq 8

$$\sum F_2 = F_{r1} + F_{b1} + F_{r2} + F_{b2} - F_{v2} \tag{8}$$

As acoustic radiation forces F_{r1} and F_{r2} and LCBE forces F_{b1} and F_{b2} are all in $+X$ and $+Y$ directions, the total force $\sum F_2$ must be in the $+XOY$ plane as well. Then, the friction force F_{v2} should point at the counter direction.

2.2.1.3. Two Counter Piezoelectric Transducers (AC1 + AC3). As shown in Figure 1e, the forces applied on the PS microparticles include acoustic radiation forces F_{r1} and F_{r3} generated by two counter piezoelectric transducers 1 and 3. Considering the viscous resistance force F_{v3}, the total force $\sum F_3$ can be calculated by eq 9 and is shown as follows

$$\sum F_3 = F_{r1} - F_{r3} - F_{v3} \text{ or } \sum F_3 = F_{r3} - F_{r1} - F_{v3} \tag{9}$$

According to eqs 1 and 2, on the left side of the pressure node, since force F_{r1} is greater than force F_{r3}, the microparticle moves along the $+X$ direction; on the right side of the pressure node, since force F_{r3} is greater than force F_{r1}, the particle moves along in the $-X$-axis.[45] As a consequence, the particles move and concentrate in nodal positions because the acoustic radiation force is generated by acoustic potential gradients that arise from the intersection of counter-propagating wavefronts.

2.2.2. Movement Analysis of Microparticles Driven by Piezoelectric Transducer (AC5/AC6) in the 3D Platform. As shown in Figure 6f, the PS particles are subjected to acoustic radiation force (F_{r5}) and viscous resistance force (F_{v4}) along the $+Z/-Z$ direction (perpendicular to the direction of the transducer) under single piezoelectric transducer T5 or T6 driving. Herein, the resultant force $\sum F_4$ can be calculated by eq 10

$$\sum F_4 = F_{r5} - F_{v4} \tag{10}$$

According to eqs 1 and 3, the PS microparticles travel in the direction of $+Z$ axis by T5 driving. Similarly, when a voltage is applied to another transducer, microparticles can move along the $-Z$ axis.

3. RESULTS AND DISCUSSIONS

3.1. Experimental Analysis of Microparticle Moving Trajectories under Different Driving Modes.
3.1.1. One Transducer Combined with One DC Electric Field (T1 + E1). To investigate the motion of PS particles in LC solutions in single BAW, single LCBE and combined fields, the driving voltages of LCBE electric field and BAW acoustic field were set as 30 V of DC voltage, 7.5 kHz of frequency, and 11 and 13 Vpp of AC voltages, respectively.

The time-displacement motion curves of PS particles are shown in Figure 2a and Table 1 under different driving modes. Displacement data versus the time were fitted with linear equation, which means the average velocity of PS microparticles. From Figure 2a, we can find that the particle moves at a small speed of 4.07 μm/s driven by single LCBE. The velocity of the particle reached 9.28 and 23.96 μm/s when AC voltages of 11 and 13 Vpp were applied on the LC solution, respectively. The results show that the manipulating effect by single BAW driving was greater than that of the single LCBE driving. In addition, under the combined BAW (13 Vpp) and LCBE (30 V) driving mode, the particle velocities can reach

35.60 and 54.82 μm/s, respectively. That was because that the resultant force between the acoustic radiation and liquid crystal backflow effect force had a positive effect to the particle motion toward the same direction ($+X$), as shown in Figure 1c, which is consistent with the theory analysis in Section 2.2.1. The displacement of the PS particles at different times (1.2, 2.4, 3.6, 4.8, 6.0, and 7.2 s) is shown in Figure 2b. The velocity of 54.821 μm/s can be calculated according to the trajectories of these images taken by the CCD camera with T1 and E1.

Here, substrate oscillations can actuate the LC fluid when the piezoelectric transducers were activated at 7.2 kHz, which will drive the suspended particle movement. This is because sub-wavelength effects with respect to an acoustic field arising in the fluid can utilize features smaller than the acoustic wavelength to modify the acoustic field,[46] which explained why particles can be manipulated using the piezoelectric transducer which produce acoustic waves larger than the particle's diameter.

3.1.2. Two Adjacent Transducers and Two DC Electric Field Driving (T1 + T2 and E1 + E2). In order to investigate the influence of two adjacent transducers combined with two LCBE electric field driving to the PS particles motion in LC solution, different driving combinations between T1, T2, E1, and E2 electric fields have been studied here. According to the theory analysis of Section 2.2, the PS particles should move in the $+XOY$ plane. The time-displacement curves of $+X$ and $+Y$ directions are shown in Figure 3a and Figure 3b with different driving mode combinations. From Figure 3a,b, we can find that when the AC voltage is equal to 13 Vpp (green line), the moving velocity of the PS particles in $+X$ and $+Y$ direction is greater than that of 11 Vpp (brown line). Thus, larger AC driving voltage will lead to larger velocity of particles in this direction, as shown in Figure 3a,b. The velocity (purple line) in $+X$ direction is larger than the red one because the 13 Vpp of driving voltage/AC1 is higher than 11 Vpp/AC2. On the contrary, the velocity of $+Y$ direction is higher than that of $+X$ direction in Figure 3b.

Similarly, E1 and E2 have the same influence on the velocity of the PS particles. As shown in Figure 3a,b, the applied E1/E2 leads to the higher velocity of the $+X/+Y$ direction. Finally, the total four electric fields are all turned on, and the velocity of PS microparticles reaches the highest value of 68.78 μm/s after calculating the velocity of $+X$ and $+Y$ directions, which point in the 45° direction in the $+XOY$ plane. Compared to the speed of 2 μm/s based on a micro-fluidic actuator developed by Liu et al, the velocity of the microparticles in this experiment has been greatly increased. The trajectories of PS particles from 0 to 7.2 s is away from the origin point, as shown in Figure 3c, by T1 and T2 combined driving. There is an increase in velocity for two similar conditions (T1 = T2 = 13 Vpp; T1 = T2 = 13 Vpp and E1 = E2 = 30 V), which is due to the presence of acoustic and electronic fields, which collectively cause the microparticles to move, such as 48.452 μm/s with T1 = T2 = 13 Vpp, E1 = E2 = 30 V driving and 24.369 μm/s with T1 = T2 = 13 Vpp driving, which represent the velocity magnitude. The moving displacement in $+X$ and $+Y$ directions increased along with the increase of time, which is consistent with the time displacement and theory analysis given in Section 2.2.

3.2. Application of Microparticle Manipulation in the 2D Platform.
3.2.1. Random Position Manipulation of PS Particles. According to the aforementioned analysis, the particle can move at any directions in the XOY plane of 2D platform if we turn on/off T1−T4 in some sequence. A single

chip microcomputer and four relays were used to control the switching sequence of four transducers connecting to the four relays through the programmable logic program. Therefore, the auto control model was designed and programmed by four relay controllers (relay 1 to relay 4 control T1 to T4, respectively), as shown in Figure 4a,b. In addition, the
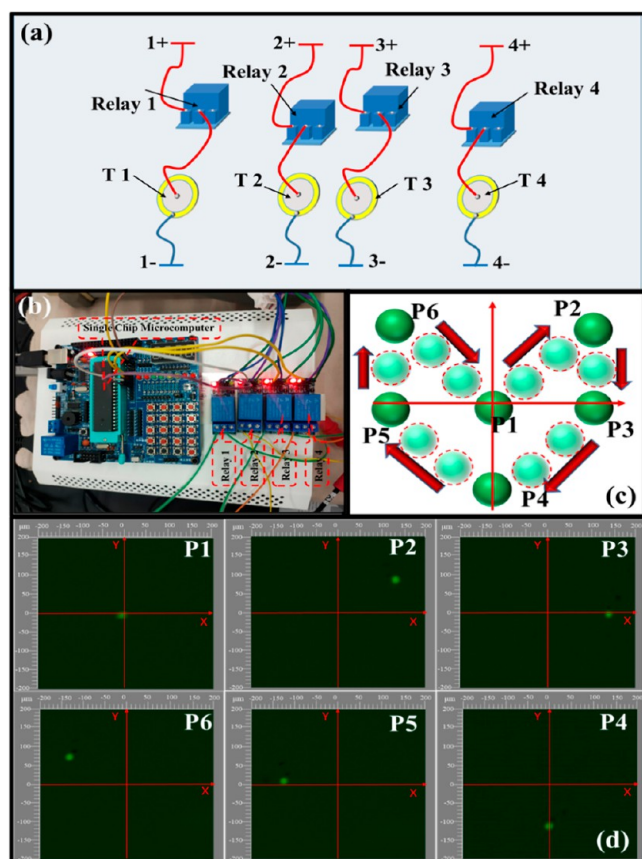
Figure 4. Analysis of random position manipulation of PS particles. (a,b) Arrangement of relay controller and piezoelectric transducer. (c) Schematic diagram of PS particles motion with a programmable logic control circuit. The trajectory of microparticle follows P1 → P2 → P3 → P4 → P5 → P6 → P1. (d) Experimental image showing motion trajectories of PS particles.

microparticle moving direction and distance will be manipulated by programmed the relay time and turn on/off in sequence between T1 and T4. For example, in order to fulfill the motion of PS particles from P1 → P2 → P3 → P4 → P5 → P6 → P1, the on/off arrangement of T1 to T4 and the relay time for four controllers were programmed as 2, 1, 2, 2, 1, and 1 s, as shown in Table 2. For example, when PS particles move from P3 to P4 position, relays 1 and 2 will turn off and relays 3

Table 2. Position of PS[a]

T/s	relay 1	relay 2	relay 3	relay 4	position
2	on	on	off	off	P1 → P2
1	off	off	off	on	P2 → P3
2	off	off	on	on	P3 → P4
2	off	on	on	off	P4 → P5
1	off	on	off	off	P5 → P6
1	on	off	off	off	P6 → P1

[a]Particles vs programmed logic control of relays combination.

and 4 will turn on, which will direct the motion of $+X$ and $-Y$ of the PS particles, as shown in Figure 4d. The relay times involve the velocity of PS particles; thus longer time (2 s) should be set when PS particles move along the 45° quadrant angle rather than along the X/Y axis (1 s).

Therefore, the position of PS particles will be controlled at any direction and positions by programming the transducers distributed in the four different directions turn on or off in subsequence and set the proper the relay time easily. This platform can be used for the directional movement of cells, drug delivery precision, and microparticle manipulation fields potentially.

3.2.2. RBCs Manipulation (T1 + T3). To demonstrate the capability of the proposed study for cells separation and gathering and other applications in biochemical field, RBC manipulation was performed with by two counter and four transducers driving in LC solution separately using the 2D platform. It can be seen from Figure 5a that the RBCs moved toward to the pressure nodes, and more cells would arrange in the pressure node line in the plane finally, as shown in Figure 5a. RBCs enriched with a line under the actuation of the resultant acoustic radiation when the driving voltage signals were loaded onto two counter transducers (T1 + T3 or T2 + T4), as shown in Figure 5b. On the left of pressure nodes, since F_{r1} was greater than F_{r3}, the particle moved along the $+X$-axis. Similarly, on the right of pressure nodes, the particle moved along the $-X$-axis, resulting in the accumulation of particles in nodal positions. The total forces of applied on the microparticle were equal to zero at the pressure node, as shown in Figure 1e. As a consequence, the particles were concentrated near the pressure nodes.

In addition, after applying four BAW signals (T1, T2, T3, and T4), it can be seen from Figure 5c,d that RBCs were concentrated at the pressure nodes in LC solution, which is consistent with the theory analysis and eq 9 in Section 2.2.1. Therefore, the RBCs and other cells with different radii can be separated and enriched together easily by BAW and/or LCBE driven using the proposed 2D platform.

3.3. Microparticle Manipulation in the 3D Platform (T5 + T6). In the 3D platform, the piezoelectric transducers T5 and T6 were placed on the counter sidewalls, which can obtain the motion of the microparticle in the Z direction. After T5 is applied at 13 Vpp voltage with 7.2 kHz driving frequency, microparticles in the 3D cavity are moving along $+Z$ direction due to acoustic radiation force generated from the transducer 5. The particle trajectory image taken in the experiment is consistent with the PS particle trajectory in 2D. The velocity of the particle reached 26.946 μm/s using the same measurements. Similarly, with T6 driven by the same electrical signal, we can obtain the trajectory of ps particles moving along the $-Z$ axis direction. The time-displacement curves of PS particles along with the $+Z$ axis are shown in Figure 6a with 13 Vpp voltage by T5 driving. The velocity can reach 26.946 μm/s according to Figure 6a. Thus, BAW based on a low frequency transducer can manipulate the motion of particles along the direction of the vertical transducer in the 5CB liquid crystals solution. However, the moving trajectories of PS particles were complex when T5 and T6 were all turned on according to multiple attempts.

In order to figure out the moving condition under T5 and T6 combined driving in the 3D platform, the FEA using COMSOL software was performed. The parameters of piezoelectric transducer are shown in Table 3 during FEA.[47]
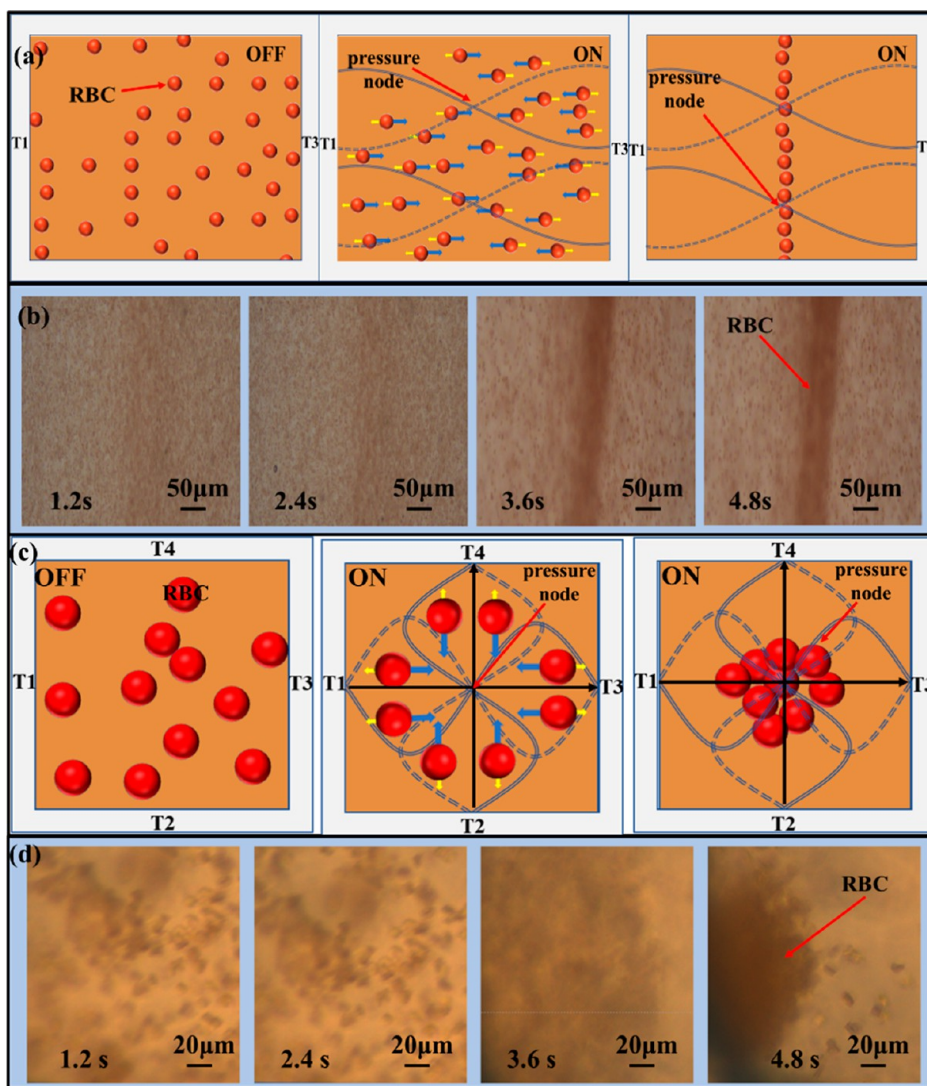
Figure 5. Manipulation of the RBCs with BAW driving. (a) Moving control of RBCs by two counter piezoelectric transducers driving in the LC solution. (b) Images of the RBCs arrangement process in the LC solution. (c) Schematic of RBCs gathering in the pressure nodes by four piezoelectric transducers driving in the LC solution. (d) Images of the gathering process of RBCs in liquid crystal solution.

As shown in Figure 6b−d, when a sine signal with 7.2 kHz driving frequency and 13 Vpp driving voltage was applied on the piezoelectric transducers T5 and T6, the direction of fluid stream is not consistent and the vortices will be formed by liquid crystals flowing, which are shown in Figure 6e−h. According to the numerical and experimental analysis, the motion of particles in the 3D plane is not easy to control, which is hard for particle manipulation. The result of numerical simulation proved to yield comparable wave patterns to the experimental results.

4. CONCLUSIONS

In this paper, a novel microparticle manipulation method based on BAW/LCBE driving is proposed. Basically, both 2D and 3D platforms with different combined driving methods were applied to manipulate PS particles and RBCs. When a single BAW field (13 Vpp voltage) and LCBE (30 V voltage) driving were applied, the velocity of PS particles can reach up to the 35.60 and 4.07 μm/s, respectively. On the other hand, the highest velocity of PS particles can reach 68.78 μm/s in the 2D platform based on a BAW (13 Vpp voltage) field combined

with LCBE (30 V voltage) driving. In addition, the microparticles in the 3D platform could be manipulated in the Z-axis direction in the LC solutions. Consequently, PS particles can be manipulated randomly in the X, Y, and Z directions through a programmable logic control model in 2D/ 3D platforms.

Finally, we demonstrated that RBCs can be enriched in a line or gathered in the pressure nodes on the actuation of acoustic waves, which can generate the two counter transducers or four transducers. Therefore, the combined driving model which solved the low driving force of single actuation mode offers new possibilities in the future studies. In the future, the dielectric anisotropy properties of liquid crystals will be introduced to manipulate particles or cells owing to potential photo-induced mechanical actuation of liquid crystals.

5. MATERIALS AND EXPERIMENT

5.1. Materials. An ultrasonic power amplifier (Nantong Longyi Electronic Technology Co. Ltd, Nantong, China), a charge-coupled device, and research-level multifunctional
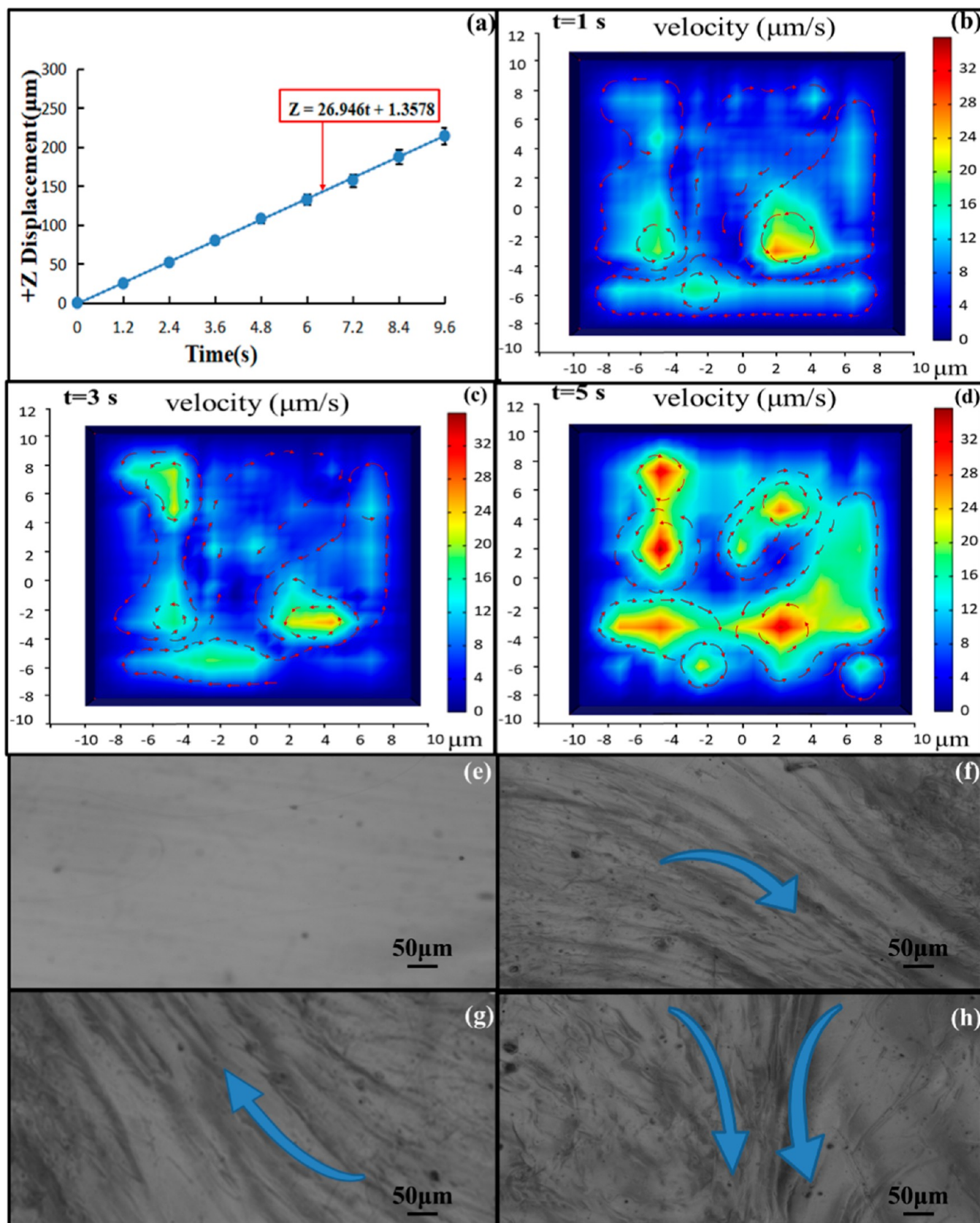
Figure 6. PS particles manipulation and vortex analysis in the 3D platform. (a) Time-displacement curves of PS particles in the +Z direction. (b−d) Vortex analysis of LC solution with two counter piezoelectric transducers in the 3D platform by FEA. (e−h) Vortices analysis observed by 5× objective magnification of CCD light field at different positions in LC solution.

Table 3. Parameter of the Piezoelectric Transducers

parameter	value
piezoelectric plate diameter D (mm)	9
piezoelectric plate thickness t (mm)	0.05
cooper substrate diameter d (mm)	12
cooper substrate thickness T (mm)	0.12
resonant frequency (kHz)	7.2 ± 0.5
impedance (Ω)	500
capacitance (nF)	$15 \pm 30\%$

intelligent microfluidic microsystem test platform (Leica Microsystems CMS GmbH) were used; 4-pentyl-4′-cyanobiphenyl (5CB) was purchased from Shijiazhuang Huarui Scientific and Technological Co. Ltd, Shijiazhuang, China); piezoelectric transducers (FT-12T-7.2A1, Tianyi Electronics, China), a signal generator (DG1022, Rigol, Zhengzhou, China), glasses (Shenzhen Micro Nano Electronic Technology Co., Ltd, China), and green fluorescent microspheres (PS) were purchased from Tianjin Sailun Technology Co.. A laser engraving machine (Liaocheng Mingchuang Laser Equipment Co., Ltd, China), an analytical Balance (Shanghai Puchun Measuring Instrument Co., Ltd, China), and a DZF-6050 vacuum dryer (Wanyi Technology Co., Ltd., Anhui, China) were purchased from their respective suppliers and used as received. Blood was collected from volunteers. All experiments were approved by the ethical committee in Henan University of Technology and are performed in compliance with the ethical policy for use of human subjects according to the national guideline in China. Informed consent was obtained for all experimentation with human subjects.

5.2. Experimental Setup. The experimental platform for microparticle manipulation is shown in Figure 7a, which mainly consists of a digital imaging computer, Leica microscopes, a power amplifier, a signal generator, and an electronic ballast switchgear. During experiments, we first connected the transducers with the output terminal of the power amplifier according to the specific experimental content. Then the amplifier was connected with a signal generator. Figure 7b shows that the 2D structure was used for PS particle

manipulation in liquid crystal flow field. It can also be used for the RBC enrichment experiment. In addition, it can be seen from Figure 7c that the 3D platform was used to investigate the motion trajectories of PS particles along with the Z axis (direction of the vertical transducers). Besides, vortices from liquid crystal flow experiments can be implemented in the 3D device.

Sample preparation: PS + LC sample solution (the mixing ratio is 1:200) and RBCs + LC sample solution (the mixing ratio is 1:200). Each experiment set in this paper was repeated five times ($n = 5$), and all the experimental data were calculated based on the mean and standard deviation (SD) and shown as mean $\pm$ SD. Alternating current (AC) with frequency of 7.2 Hz, 11, 13 peak-to-peak voltage (Vpp) and direct current (DC) with 30 V were used in all experiments. This is due to evident microparticle movement trajectory observed by sweeping the voltages with 1 Vpp increment from 1 to 30 Vpp.

■ AUTHOR INFORMATION

Corresponding Authors

Yanfang Guan − School of Electromechanical Engineering, Henan University of Technology, Zhengzhou 450001, China; National Engineering Laboratory/Key Laboratory of Henan Province, Henan University of Technology, Zhengzhou 450001, China; ⊙ orcid.org/0000-0001-5615-5077; Email: yguan@haut.edu.cn

Ronghan Wei − Nano Opto-mechatronics & Biomedical Engineering Lab, Zhengzhou University, Zhengzhou 450001, China; Email: frofessorwei@163.com

Authors

Xiaoliang Wang − School of Electromechanical Engineering, Henan University of Technology, Zhengzhou 450001, China

Guangyu Liu − School of Electromechanical Engineering, Henan University of Technology, Zhengzhou 450001, China

Wujie Li − School of Electromechanical Engineering, Henan University of Technology, Zhengzhou 450001, China

Kun Zhang − School of Electromechanical Engineering, Henan University of Technology, Zhengzhou 450001, China
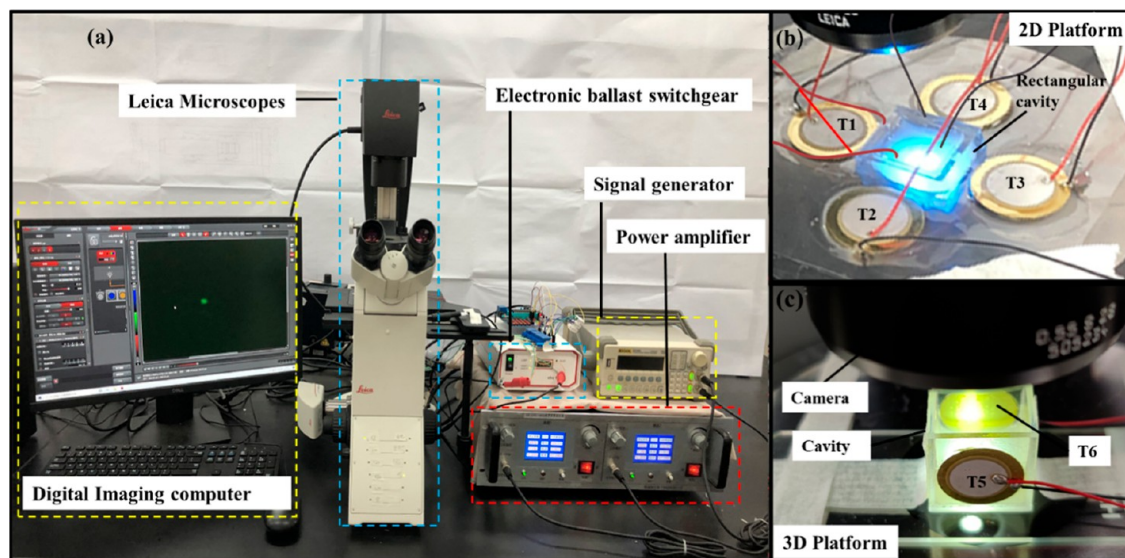
Figure 7. Experimental setup for microparticle manipulation. (a) Overall setup of the microparticle manipulation platform. (b,c) Photos of the working area for the 2D platform and 3D platform.

Baoshuo Sun − *School of Electromechanical Engineering, Henan University of Technology, Zhengzhou 450001, China*

Feifan Shi − *School of Electromechanical Engineering, Henan University of Technology, Zhengzhou 450001, China*

Yanbo Hui − *School of Electromechanical Engineering, Henan University of Technology, Zhengzhou 450001, China*

Bingsheng Yan − *School of Electromechanical Engineering, Henan University of Technology, Zhengzhou 450001, China*

Jie Xu − *Mechanical and Industrial Engineering, University of Illinois at Chicago, Chicago, Illinois 60607, United States*

Zaihui Wu − *Zhengzhou Institute of Biomedical Engineering and Technology, Zhengzhou 450001, China*

Zhiyong Duan − *Nano Opto-mechatronics & Biomedical Engineering Lab, Zhengzhou University, Zhengzhou 450001, China*

Complete contact information is available at:
https://pubs.acs.org/10.1021/acsomega.2c01783

Author Contributions

Y.F.G. designed the study. X.L.W. performed the experiments. Y.F.G. and X.L.W. wrote the paper. Y.F.G. reviewed and edited the manuscript. B.S.S., F.F.S., W.S.L., and G.Y.L. performed the experiments. Y.B.H., J.X., B.S.Y., Z.H.W., Z.Y.D., and R.H.W. performed the simulations. The manuscript was written through contributions of all authors. All authors have given approval to the final version of the manuscript.

Notes

The authors declare no competing financial interest.

■ REFERENCES

(1) Chin, C. D.; Linder, V.; Sia, S. K. Commercialization of microfluidic point-of-care diagnostic devices. *Lab Chip* **2012**, *12*, 2118−2134.

(2) Bachman, H.; Chen, C.; Rufo, J.; Zhao, S.; Yang, S.; Tian, Z.; Nama, N.; Huang, P.-H.; Huang, T. J. An acoustofluidic device for efficient mixing over a wide range of flow rates. *Lab Chip* **2020**, *20*, 1238−1248.

(3) Simon, G.; Andrade, M. A. B.; Reboud, J.; Marques-Hueso, J.; Desmulliez, M. P. Y.; Cooper, J. M.; Riehle, M. O.; Bernassau, A. L. Particle separation by phase modulated surface acoustic waves. *Biomicrofluidics* **2017**, *11*, 054115.

(4) Liu, P.; Tian, Z.; Hao, N.; Bachman, H.; Zhang, P.; Hu, J.; Huang, T. J. Acoustofluidic multi-well plates for enrichment of micro/nano particles and cells. *Lab Chip* **2020**, *20*, 3399−3409.

(5) Yang, C.-G.; Xu, Z.-R.; Wang, J.-H. Manipulation of droplets in microfluidic systems. *TrAC, Trends Anal. Chem.* **2010**, *29*, 141−157.

(6) Faridi, M. A.; Ramachandraiah, H.; Iranmanesh, I.; Grishenkov, D.; Wiklund, M.; Russom, A. MicroBubble activated acoustic cell sorting. *Biomed. Microdevices* **2017**, *19*, 23.

(7) Dow, P.; Kotz, K.; Gruszka, S.; Holder, J.; Fiering, J. Acoustic separation in plastic microfluidics for rapid detection of bacteria in blood using engineered bacteriophage. *Lab Chip* **2018**, *18*, 923−932.

(8) Fan, X.; White, I. M. Optofluidic Microsystems for Chemical and Biological Analysis. *Nat. Photonics* **2011**, *5*, 591−597.

(9) Sidelman, N.; Cohen, M.; Kolbe, A.; Zalevsky, Z.; Herrman, A.; Richter, S. Rapid Particle Patterning in Surface Deposited Micro-Droplets of Low Ionic Content via Low-Voltage Electrochemistry and Electrokinetics. *Sci. Rep.* **2015**, *5*, 13095.

(10) Lebel, P.; Basu, A.; Oberstrass, F. C.; Tretter, E. M.; Bryant, Z. Gold rotor bead tracking for high-speed measurements of DNA twist, torque and extension. *Nat. Methods* **2014**, *11*, 456−462.

(11) Zhang, P.; Bachman, H.; Ozcelik, A.; Huang, T. J. Acoustic Microfluidics. *Annu. Rev. Anal. Chem.* **2020**, *13*, 17−43.

(12) Liu, G.; He, F.; Li, Y.; Zhao, H.; Li, X.; Tang, H.; Li, Z.; Yang, Z.; Zhang, Y. Effects of two surface acoustic wave sorting chips on particles multi-level sorting. *Biomed. Microdevices* **2019**, *21*, 59.

(13) Friend, J.; Yeo, L. Y. Microscale acoustofluidics: Microfluidics driven via acoustics and ultrasonics. *Rev. Mod. Phys.* **2011**, *83*, 647−704.

(14) Wu, M.; Ozcelik, A.; Rufo, J.; Wang, Z.; Fang, R.; Jun Huang, T. Acoustofluidic separation of cells and particles. *Microsyst. Nanoeng.* **2019**, *5*, 32.

(15) Guan, Y.; Sun, B. Versatile Microfluidic Mixing Platform for High- and Low-Viscosity Liquids via Acoustic and Chemical Microbubbles. *Micromachines* **2019**, *10*, 854.

(16) Schmid, L.; Wixforth, A.; Weitz, D. A.; Franke, T. Novel surface acoustic wave (SAW)-driven closed PDMS flow chamber. *Microfluid. Nanofluidics* **2011**, *12*, 229−235.

(17) Liu, G.; He, F.; Li, X.; Zhao, H.; Zhang, Y.; Li, Z.; Yang, Z. Multi-level separation of particles using acoustic radiation force and hydraulic force in a microfluidic chip. *Microfluid. Nanofluidics* **2019**, *23*, 23.

(18) Xie, Y.; Rufo, J.; Zhong, R.; Rich, J.; Li, P.; Leong, K. W.; Huang, T. J. Microfluidic Isolation and Enrichment of Nanoparticles. *ACS Nano* **2020**, *14*, 16220.

(19) Xie, Y.; Mao, Z.; Bachman, H.; Li, P.; Zhang, P.; Ren, L.; Wu, M.; Huang, T. J. Acoustic Cell Separation Based On Biophysical Properties. *J. Biomech. Eng.* **2020**, *142*, 0310051.

(20) Settnes, M.; Bruus, H. Forces acting on a small particle in an acoustical field in a viscous fluid. *Phys. Rev. E: Stat., Nonlinear, Soft Matter Phys.* **2012**, *85*, 016327.

(21) Dai, H.; Liu, L.; Xia, B.; Yu, D. Experimental Realization of Topological On-Chip Acoustic Tweezers. *Phys. Rev. Appl.* **2021**, *15*, 064032.

(22) Yu, Y.; Wang, Q.; Wang, C.; Shang, L. Living Materials for Regenerative Medicine. *Eng. Regen.* **2021**, *2*, 96−104.

(23) Yang, C.; Yu, Y.; Wang, X.; Wang, Q.; Shang, L. Cellular fluidic-based vascular networks for tissue engineering. *Eng. Regen.* **2021**, *2*, 171−174.

(24) Wu, M.; Ouyang, Y.; Wang, Z.; Zhang, R.; Huang, P.-H.; Chen, C.; Li, H.; Li, P.; Quinn, D.; Dao, M.; Suresh, S.; Sadovsky, Y.; Huang, T. J. Isolation of exosomes from whole blood by integrating acoustics and microfluidics. *Proc. Natl. Acad. Sci. U. S. A.* **2017**, *114*, 10584−10589.

(25) Zhang, P.; Wang, W.; Fu, H.; Rich, J.; Su, X.; Bachman, H.; Xia, J.; Zhang, J.; Zhao, S.; Zhou, J.; Huang, T. J. Deterministic droplet coding via acoustofluidics. *Lab Chip* **2020**, *20*, 4466−4473.

(26) Lee, K.; Shao, H.; Weissleder, R.; Lee, H. Acoustic purification of extracellular microvesicles. *ACS Nano* **2015**, *9*, 2321−2327.

(27) Bachman, H.; Gu, Y.; Rufo, J.; Yang, S.; Tian, Z.; Huang, P.-H.; Yu, L.; Huang, T. J. Low-frequency flexural wave based microparticle manipulation. *Lab Chip* **2020**, *20*, 1281−1289.

(28) Koide, N. *The Liquid Crystal Display Story‖Modes for Liquid Crystal Devices*; Springer Japan, 2014; Chapter 6, pp 131−170.

(29) Liu, C.; Li, B.; Guan, Y.; Wang, A. Experimental study of the microfluidic driving based on the liquid crystalline backflow effect. *Ying Yong Li Xue Xue Bao* **2019**, 135−140 (In Chinese).

(30) Guan, Y. Performance Analysis of a Microfluidic Pump Based on Combined Actuation of the Piezoelectric Effect and Liquid Crystal Backflow Effect. *Micromachines* **2019**, *10*, 584.

(31) Liu, C. Fundamental Study on New Micro Fluidic Drive Method Based on Liquid Crystalline Backflow. *Res. J. Appl. Sci. Eng. Technol.* **2012**, *4*, 4825−4829.

(32) Zhang, X.; Sun, L.; Wang, Y.; Bian, F.; Wang, Y.; Zhao, Y. Multibioinspired slippery surfaces with wettable bump arrays for droplets pumping. *Proc. Natl. Acad. Sci. U. S. A.* **2019**, *116*, 20863−20868.

(33) Wang, H.; Cai, L.; Zhang, D.; Shang, L.; Zhao, Y. Responsive Janus Structural Color Hydrogel Micromotors for Label-Free Multiplex Assays. *Research* **2021**, *2021*, 9829068.

(34) Yang, H.-H.; Han, C.-H.; Lee, J. O.; Yoon, J.-B. Electrostatic micro-actuator with a pre-charged series capacitor: modeling, design, and demonstration. *J. Micromech. Microeng.* **2014**, *24*, 065012.

(35) Chakraborty, J.; Ray, S.; Chakraborty, S. Role of streaming potential on pulsating mass flow rate control in combined electroosmotic and pressure-driven microfluidic devices. *Electrophoresis* **2012**, *33*, 419−425.

(36) Zhang, X. Y.; Uchiyama, K.; Ishizuka, T. High-Speed, High-Precision Magnetic/Piezoelectric Hybrid Drive Actuator for Micro Electrical Discharge Machining. *Adv. Mater. Res.* **2014**, *941−944*, 2112−2115.

(37) Kang, P.; Tian, Z.; Yang, S.; Yu, W.; Zhu, H.; Bachman, H.; Zhao, S.; Zhang, P.; Wang, Z.; Zhong, R.; Huang, T. J. Acoustic tweezers based on circular, slanted-finger interdigital transducers for dynamic manipulation of micro-objects. *Lab Chip* **2020**, *20*, 987−994.

(38) Wu, M.; Huang, P. H.; Zhang, R.; Mao, Z.; Chen, C.; Kemeny, G.; Li, P.; Lee, A. V.; Gyanchandani, R.; Armstrong, A. J.; Dao, M.; Suresh, S.; Huang, T. J. Circulating Tumor Cell Phenotyping via High-Throughput Acoustic Separation. *Small* **2018**, *14*, No. e1801131.

(39) Orbay, S.; Ozcelik, A.; Lata, J.; Kaynak, M.; Wu, M.; Huang, T. J. Mixing high-viscosity fluids via acoustically driven bubbles. *J. Micromech. Microeng.* **2017**, *27*, 015008.

(40) Zhou, J.; Habibi, R.; Akbaridoust, F.; Neild, A.; Nosrati, R. Paper-Based Acoustofluidics for Separating Particles and Cells. *Anal. Chem.* **2020**, *92*, 8569−8578.

(41) Wang, X.; Chen, S.; Kong, M.; Wang, Z.; Costa, K. D.; Li, R. A.; Sun, D. Enhanced cell sorting and manipulation with combined optical tweezer and microfluidic chip technologies. *Lab Chip* **2011**, *11*, 3656−3662.

(42) Skowronek, V.; Rambach, R. W.; Schmid, L.; Haase, K.; Franke, T. Particle deflection in a poly(dimethylsiloxane) microchannel using a propagating surface acoustic wave: size and frequency dependence. *Anal. Chem.* **2013**, *85*, 9955−9959.

(43) Shields, C. W.; Reyes, C. D.; López, G. P. Microfluidic cell sorting: a review of the advances in the separation of cells from debulking to rare cell isolation. *Lab Chip* **2015**, *15*, 1230−1249.

(44) Muller, P. B.; Barnkob, R.; Jensen, M. J. H.; Bruus, H. A numerical study of microparticle acoustophoresis driven by acoustic radiation forces and streaming-induced drag forces. *Lab Chip* **2012**, *12*, 4617−4627.

(45) Shi, J.; Huang, H.; Stratton, Z.; Huang, Y.; Huang, T. J. Continuous particle separation in a microfluidic channel via standing surface acoustic waves (SSAW). *Lab Chip* **2009**, *9*, 3354−3359.

(46) Kolesnik, K.; Xu, M.; Lee, P. V. S.; Rajagopal, V.; Collins, D. J. Unconventional acoustic approaches for localized and designed micromanipulation. *Lab Chip* **2021**, *21*, 2837−2856.

(47) Guan, Y.; Li, X. Analysis of Vibrational Performance of A Piezoelectric Micropump with Diffuse/Nozzle Microchannel. *Nanotechnol. Precis. Eng.* **2018**, *1*, 138.